MICROCRACK STRUCTURE AND ITS EFFECT ON ELECTRICAL CONDUCTIVITY

Frank D. Börner, Dresden Groundwater Research Centre, Dresden, Germany
Jürgen H. Schön; Joanneum Research Centre, Leoben, Austria

Abstract
The frequency dependence of complex electrical conductivity in the frequency range from 10^{-3} to 10^3 Hertz has been investigated for a variety of microcracked rocks from the German continental deep drilling project (KTB), Northern Bavaria. The laboratory measurements were made with a computer controlled four-electrode system on plugs saturated with brine of different salinity. It has been found that the complex electrical conductivity may be described using well known models applied for shaly sands. The main feature of the conductivity spectra is a constant phase angle over the investigated frequency range combined with a nearly identical power law frequency dependence of the real as well as the imaginary parts. The results of the study show that complex electrical parameters dependent on (1) the crack porosity and surface area to porosity ratio, (2) the conductivity and other properties of the crack filling water, and (3) orientation and genesis of the microcrack network. Complex conductivity measurements allow an uncomplicated separation of electrical volume and interface effects. Moreover, the results suggest that determination of specific surface area and other microcrack network characteristics of crystalline rocks directly from complex electrical measurements can be made.

Introduction
Crystalline and metamorphic rocks are generally heterogeneous multiphase systems with a complicated internal microcrack system. They consist mainly of a nonconductive silicate matrix and a more or less conductive electrolyte solution in the microcrack space (Schön 1990). Various electrical phase boundary phenomena are of special interest, because they result in a dispersion of the electrical conductivity in the very low frequency range below 1 kHz. In the bench scale complex electrical parameters of crystalline rocks depend on

- mineral composition (electronic conductors),
- crack space structure (porosity, tortuosity, constrictivity),
- water composition and
- electrochemical structure of the matrix-water-interface.

Therefore, they contain information about small scale electrical and hydraulic anisotropy, permeability and fluid properties. The anisotropy is caused by the orientation of disperse or laminar conductive minerals if present, and of the water filled microcrack system. Conductive matrix components (especially graphite and sulphides) can reach high concentrations in metamorphic rocks, and the influence of these minerals on the complex conductivity is very high. But in order to avoid this additional complication, the present investigation is constricted to rocks without metallic conduction. Laboratory investigations of complex conductivity related to microstructure crystalline rocks are published for example by Olhoeft (1981), Lockner and Byerlee (1985), Kulenkampff et al. (1993), Nover and Will (1991) and Börner and Schön (1995). Of special interest is the publication related to shaly sands of Vinegar and Waxman (1984). The purpose of this paper is to provide a preliminary insight into the influence of microcrack structure upon very low frequency complex conductivity and electrical anisotropy effects in crystalline rocks.

Conductivity model

The frequency dependence of complex rock conductivity σ^* is analyzed using the constant phase angle model (Jonscher 1981, Börner, Schön, 1991, 1995):

$$\sigma^*(\omega) = \sigma_n (i\omega_n)^{1-p} \tag{1}$$

where σ_n is the conductivity amplitude at ω=1Hz, ω_n the normalized angular frequency (ω_n=ω/ω =1 Hz) and *1-p* the frequency exponent (in the order of 0 to 0.05). Generally all investigated samples without conductive matrix components (pyrite, graphite) show within a considerably error range the described frequency behaviour. Equation (1) implies a frequency dependent real and imaginary part. The existence of a separate frequency independent conductivity component is ignored because it is experimentally not clearly observeable. On the other hand interface conductivity is the dominating conductivity contribution in crystalline rocks with a nonconductive silicate matrix at medium salinities. Equation (1) may be separated into the real and imaginary component

$$\sigma'_n = \sigma_n \cos\left[\frac{\pi}{2}(1-p)\right] \text{ and } \sigma''_n = \sigma_n \sin\left[\frac{\pi}{2}(1-p)\right] \tag{2}$$

σ'_n and σ''_n are the amplitude factors of the real and the imaginary parts. Equation (2) leads to the relationship between the frequency exponent 1-p, the phase angle φ and the amplitude factors σ'_n and σ''_n:

$$\tan\varphi = \frac{\sigma''(\omega)}{\sigma'(\omega)} = \frac{\sigma''_n}{\sigma'_n} = \tan\left[\frac{\pi}{2}(1-p)\right] \tag{3}$$

For better understanding of the conductivity dispersion the relationship between the parameters in equation (2) and some microcrack and fluid properties has been analysed.

Table 1 Sample specification (selected samples).

Sample	Depth in m (KTB)	Lithology	Φ (-)	Standard deviation	S_{por} in μm^{-1}
861C2k	3518.3	Garnet-Sillimanit-Biotit-Gneiss	0.00864	0.00019	26.9
54D7m	379.9	Gneiss, mylonitic	0.0119	0.00182	9.9
23A2t	162.5	Amphibolite	0.00673	0.00015	58.0
26C1b	186.8	Amphibolite	0.00939	0.00027	69.5
294C1j	1412.8	Meta-Ultramafitite	0.00537	0.00063	0.6
940D1nk	3839.2	Garnet-Biotit-Hornblende-Gneiss	0.00422	0.00010	19.6
619A1a	2544.2	Garnet-Biotit-Hornblende-Gneiss	0.00570	0.00059	13.4
776 D1	3174.2	altered Garnet-Sillimanit-Biotit-Gneiss	-	-	-
105A1	565.6	Disthen-Sillimanit-Garnet-Biotit-Gneiss	0.00703	0.00025	58.0
GU	-	Garnet-Hornblende-Gneiss	0.00742	0.00179	82.0
UG	-	Biotit-Plagioclas-Gneiss	0.00709	0.00006	54.0

Experimental

Complex conductivity measurements were made on a series of different crystalline rock samples from the 4000 m deep KTB-pilot hole and some other locations. The sample specification including depth of sampling can be seen in Table 1. The porosity Φ and the surface to porosity ratio S_{por}) have been used to characterize the material . Porosity was measured by water injection on samples with a defined geometry. Internal surface area S_m was determined by using BET-nitrogen-adsorption. The parameter S_{por} is important for characterizing Transport properties of rocks (Pape et. al 1987). All samples were carefully vacuum saturated with sodium chloride solution of known conductivity σ_w at 25°C after drying at 60°C to a constant weight. The conductivity of the brine was in the range from 0.001 to 10 S/m.

Relationship to surface area and porosity

Surface area, porosity and tortuosity are important parameters for the characterization of microfracture geometry. Hence it is necessary to understand how these quantities control the level of complex conductivity components, and therefore induced polarization-parameters derived from logs.

The experimental investigation of salinity dependence of complex conductivity components (multiple salinity method) has shown a similar behaviour to shaly sands. The real part σ'_n in equation (2) can be divided into an electrolytical volume conductivity component σ_{el} and an ohmic interface conductivity component σ'_i, corresponding to the expressions of Waxman and Smits (1968) and Rink and Schopper (1974) for fixed frequency measurements:

$$\sigma'_n = \sigma_{el} + \sigma'_i \tag{4}$$

σ_{el} with the well known Archie-equation (Archie, 1942)

$$\sigma_{el} = \sigma_w / F \tag{5}$$

where σ_w is the water conductivity and F the high salinity formation factor. Solid-fluid-interaction between silicate matrix and brine results in the development of an electrical double layer. The capacitive behaviour of the porous multiphase system is caused by charge separation on constriction along the pore or crack throughts. Hence, the imaginary part σ''_n in equation (2) is identified with the capacitive effect of the interface σ''_i in the low frequency range:

$$\sigma''_n = \sigma''_i \tag{6}$$

The salinity dependence of σ''_i is more or less weak. The salinity dependence of both the real and imaginary part of conductivity in Figure 1 illustrates the different dependences. The experimental results in Figure 2 show that both interface conductivity components are linear dependent on S_{por} (Börner, Schön and Jung 1993). The effect was already obseved on shaly sandstones (Börner and Schön, 1991). Figure 3 illustrates the relationship between F and crack porosity. The correlation is less significant than in the case of reservoir rocks due to measurement accuracy of low porosities. Based on Rink and Schopper's (1974) equation, σ'_i is described as

$$\sigma'_i = f(\sigma_w) S_{por} / F \tag{7}$$

Table 2 Electrical parameters of crystalline rocks from the KTB-Pilot hole,

Sample	σ_w *in* S/m	σ_n	*1-p*	F
861C2k/ra1	0.00115	0.000194	0.00820	1776
861C2k/ra1	0.043	0.000214	0.00922	1776
861C2k/ra1	6.50	0.00387	0.00156	1776
861C2k/ra2	0.00298	0.000192	0.00696	1019
861C2k/ra2	0.0432	0.000317	0.00606	1019
861C2k/ra2	6.5	0.00665	0.00102	1019
776 D1 ax	0.018	0.000420	0.00386	1174
776 D1 ax	6.5	0.00594	0.00039	1174
776 D1 ra	0.018	0.000050	0.00827	1919
776 D1 ra	6.5	0.00343	0.000397	1919
54D7m/ax2	6.50	0.00651	0.00256	1031
26C1b/ra3	7.80	0.00772	0.00242	1142
294C1j	6.50	0.00303	0.00057	2143
940D1nk	0.390	0.000203	0.00815	1217
619A1a/ax	0.010	0.000109	0.00584	4367
619A1a/ra	7.8	0.00189	0.00138	-
105A1	6.5	0.0116	0.00234	591
GU/ra1	0.0284	0.000830	0.00558	970
GU/ra1	6.5	0.00749	0.00171	970
GU/ax1	0.0430	0.000428	0.00302	1840
GU/ax1	6.5	0.00394	0.00099	1840
GU/ax2	0.0305	0.000281	0.00494	1362
GU/ax2	6.5	0.00503	0.00116	1362
UG/ax	0.0132	0.000158	0.0331	3165
UG/ax	7.7	0.00259	0.0152	3165
UG/ra	0.0132	0.000307	0.0391	1754
UG/ra	7.7	0.00469	0.0156	1754

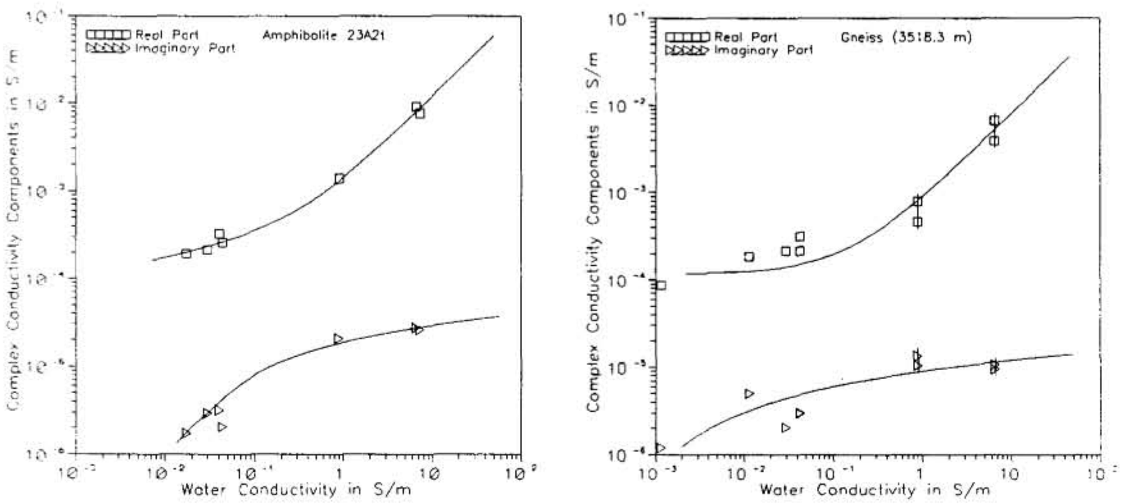

Figure 1 Real and imaginary part vs. σ_W for a gneiss and an amphibolite sample.

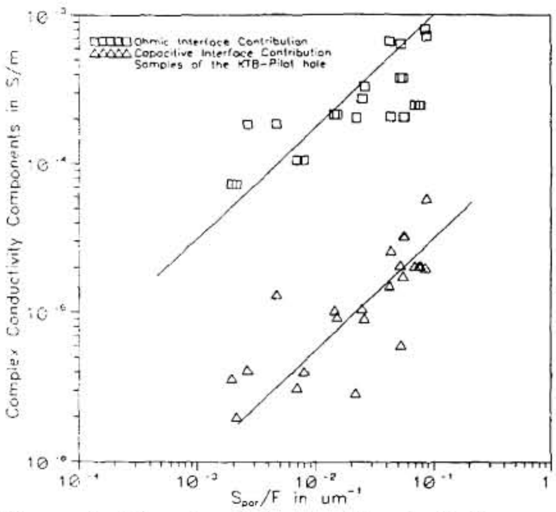

Figure 2 Complex Interface Conductivity Components vs. Surface-to-Porosity ratio S_{por}.

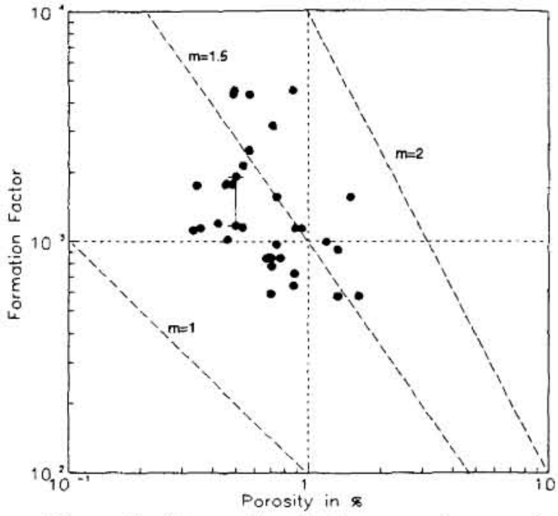

Figure 3 Formation factor vs. microcrack Porosity.

where F, for purposes of simplicity, is the same formation factor as in equation (5). $f(\sigma_W)$ is a general function considering salinity dependence (Vinegar and Waxman, 1984). The imaginary part of conductivity of gneisses and amphibolithes is described with the following simple parameter equation (see Vinegar and Waxman, 1984, Börner and Schön, 1995):

$$\sigma_i'' = lf(\sigma_w) S_{por} / F \tag{8}$$

where l is the ratio of the two interface conductivity components σ_i' and σ_i''. l is in the order of about 0.03 for the low porosity crystalline rocks. Generally, in the case of the investigated metamorphic and igneous rocks no significant difference to the complex conductivity behaviour of shaly sands was found.

Anisotropy

It is well known that metamorphic rocks are characterized by a significant anisotropy of transport properties. The orientation of conductive solid and/or liquid phases in the rock results in an electrical anisotropy. Various authors found on samples from the KTB-project an electrical anisotropy caused by microcrack orientation (e.g. Rauen and Lastovickova, 1995). But they restricted their investigation on DC-conductivity or the real component of electrical conductivity.
Microcrack networks in crystalline rock samples are generated by two different processes: true or primary microcracks are caused by tectonic stress and other geodynamic processes. The second type of microcracks is caused while the drilling and sampling process.

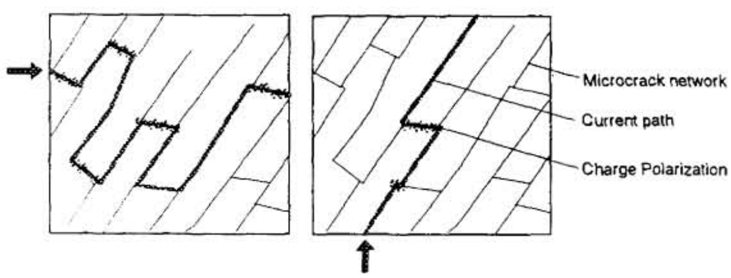

Figure 4 Anisotropy of current flow and charge polarization through the microcrack network.

We found within the investigated KTB samples an anisotropy behaviour for both the real as well as the imaginary part of conductivity (see the illustration of the effect in figure 4). In clean silicate crystalline rocks electrical anisotropy is caused by the water filled crack system alone. This anisotropy phenomenon may be separated in two types:

- orientation of the conductive crack or pore system
- orientation of the crack surface system.

The following model consideration connects measured parameters and the individual physical components of anisotropy. Equations (4) and (6) may be established for two directions (⊥ and //) of current flow though the rock. Then the anisotropy factors for the real part w_{re} as well as the imaginary part w_{im} was defined according to Schön (1996):

$$w^2_{re} = \frac{\sigma'_{el//} + \sigma'_{i//}}{\sigma'_{el\perp} + \sigma'_{i\perp}} \tag{9}$$

$$w^2_{im} = \frac{\sigma''_{i//}}{\sigma''_{i\perp}} = \frac{l_{//}\sigma'_{i//}}{l_{\perp}\sigma'_{i\perp}} \tag{10}$$

w is in order of 1.2 to 1.9 for the real part and 0.9 to 1.6 for the imaginary part. The anisotropy factors found to be dependent on frequency (figure 5). According to equation (1) the complex anisotropy **P*** is defined with:

$$P^*(\omega) = \frac{\sigma_{n//}}{\sigma_{n\perp}}(i\omega)^{p_\perp - p_{//}} \tag{11}$$

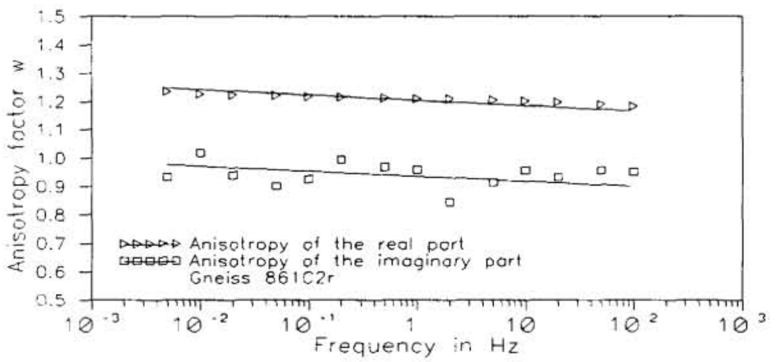

Figure 5
Frequency dependence of electrical anisotropy .

The electrical anisotropy is related to the orientation of conductive microcrack systems. It is caused by direction dependent tortuosity of crack space and crack surface. From equations (9) and (10) a relationship for the two anisotropy ratios results

$$\mathrm{W} = \frac{w^2_{im}}{w^2_{re}} = \frac{l_{\perp}}{l_{//}} \frac{\sigma'_{el\perp}\sigma'_{i//} + \sigma'_{i//}\sigma'_{i\perp}}{\sigma'_{el//}\sigma'_{i\perp} + \sigma'_{i//}\sigma'_{i\perp}} \tag{12}$$

With $\sigma'_{el\perp} = \frac{\sigma_w}{F_{\perp}} + \sigma'_{i\perp}$ and $\sigma'_{el//} = \frac{\sigma_w}{F_{//}} + \sigma'_{i//}$

equation (12) has the form

$$W = \frac{w_{im}^2}{w_{re}^2} = \frac{l_\perp}{l_{//}} \frac{\frac{1}{F_\perp} + 2\frac{\sigma'_{i\perp}}{\sigma_w}}{\frac{1}{F_{//}}\frac{\sigma'_{i\perp}}{\sigma'_{i//}} + 2\frac{\sigma'_{i\perp}}{\sigma_w}} \tag{13}$$

Equation (13) describes the dependence of the anisotropy ratio W on the pore space geometric parameters $l_\perp, l_{//}, F_\perp, F_{//}$ and the conductivity components $\sigma'_{i\perp}, \sigma'_{i//}$ depending on the orientation and the influence of the brine conductivity σ_w. Figure 6 shows curves calculated after equation (13) for different values of the individual parameters (Table 3) in a W vs. σ_w plot.

Table 3 Values for parameters in equation 13 used for figure 8.

curve in figure 6	$\frac{l_\perp}{l_{//}}$	$F_\perp$	$F_{//}\frac{\sigma'_{i//}}{\sigma'_{i\perp}}$	$2\sigma'_{i\perp}$
1	1	1000	1000	10^{-5} mS/m
2	1	1000	1430	10^{-5} mS/m
3	1	1430	1000	10^{-5} mS/m
4	1.2	1000	1430	10^{-5} mS/m
5	0.8	1430	1000	10^{-5} mS/m

Obviously there are three "types of dependence"

- W increases with increasing σ_W,
- W decreases with increasing σ_W,
- W is constant with increasing σ_W.

An analyse of the influence factors acting on anisotropy seems possible:

- the W-value for decreasing σ_w tends towards the constrictivity ratio
- the relationship between $F_\perp$ and $F_{//}(\sigma'_{i\perp} / \sigma'_{i//})$ can be derived from the character of the plot (upgoing, constant, or downgoing).

In figure 7 some experimental results are analyzed by an iterative approximation. We find all three types. The parameters are summarized in table 4.

This first test was made with a constant value for $\sigma'_{i\perp} = 0.5*10^{-05} mS/m$. The derived values confirm distinct differences of the samples with respect to the anisotropy of the constrictivity (from 0.33 to 1.43) but also to the combined effect of the anisotropy of formation factor and the ration $\sigma'_{i//} / \sigma'_{i\perp}$. A separation of the formation factor anisotropy is possible from an analyse of w_{re}^2 for high salinity:

$$w_{re}^2 = \frac{F_{//}}{F_\perp} \tag{14}$$

Table 4 Values for parameters in equation 14 obtained from experiments.

curve in figure 7	$\frac{l_{\perp}}{l_{//}}$	$F_{\perp}$	$F_{//}\frac{\sigma'_{i//}}{\sigma'_{i\perp}}$	$2\sigma'_{i\perp}$
1	0.85	1000	1730	10^{-5} mS/m
2	0.33	2000	6250	10^{-5} mS/m
3	1.43	1430	1000	10^{-5} mS/m
4	0.73	1000	900	10^{-5} mS/m

Thus the following way for a complete analyse results:

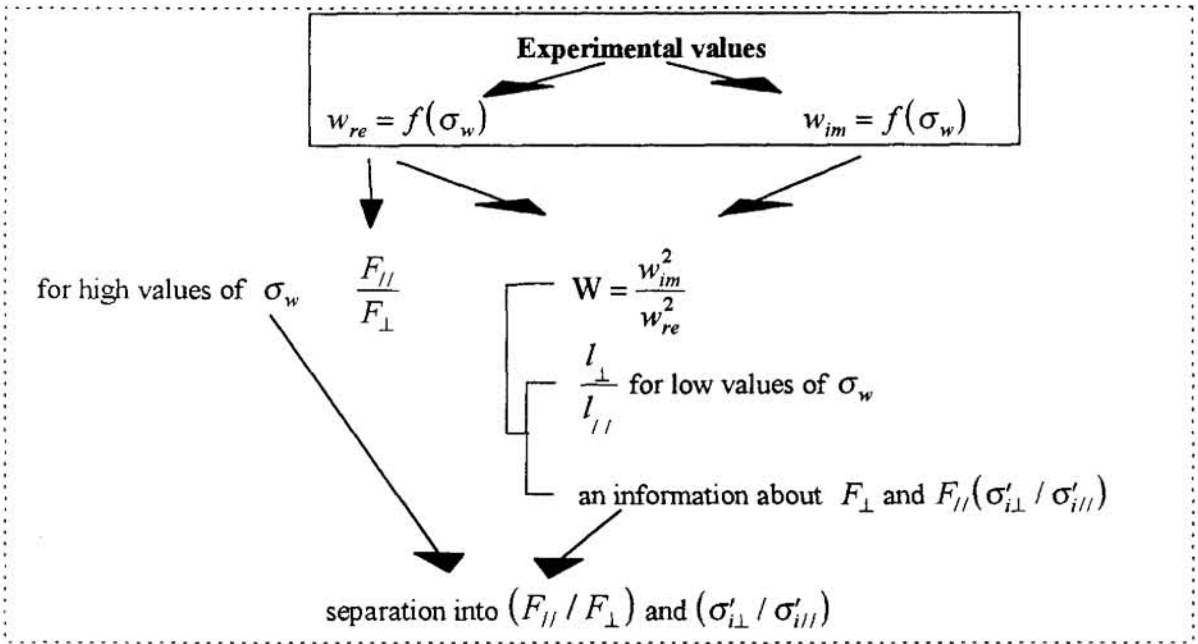

It can be seen that the ratio of the anisoptropy factors may be used to estimate the constrictivity ratio. Then we get two structural information from complex electrical anisotropy. Based on the assumption that cracks with different genesis are characterized by high and low specific surface area due to geochemical history, a differentiation seems to be possible. If the crack surface area in one direction is high the rock should have a ratio W which is significantly different from 1. In the other case, secondary cracks should be visible by a W-ratio near 1 because both anisotropy factors mainly effected by the formation factors. But further investigation are necessary.

Table 5 Values of electrical anisotropy for crystalline rocks

Type of samples	w_{re}	w_{im}
Amphibolite (KTB, this investigation)	1.08 - 1.12	1.03 - 1.29
Gneiss (KTB, this investigation)	1.22 - 2.89	1.01 - 1.97
Granite (this investigation)	1.22 - 1.72	1.36 - 1.90
Granite (Pham et. al 1995)	1.00 - 1.10	-
Gneiss (KTB, Rauen, Lastov. 1995)	2.84	-
Amphibolite	1.33	-

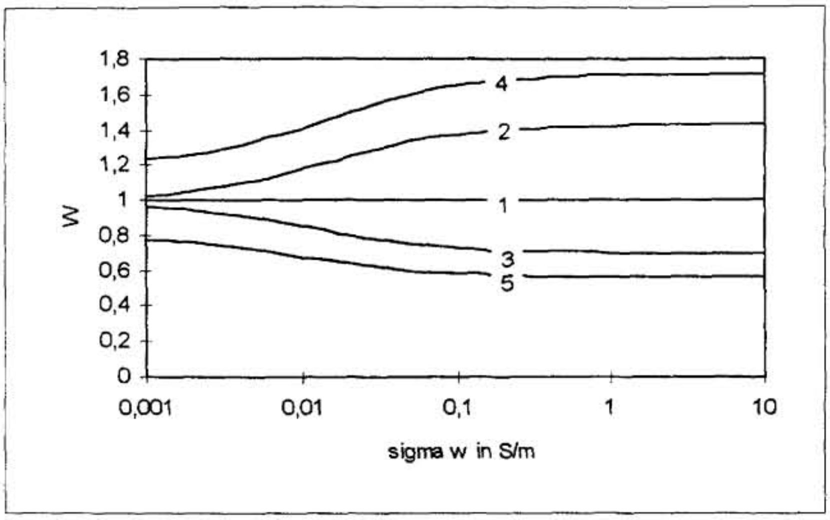

Figure 6 Anisotropy ratio W vs. water conductivity, theoretical curves.

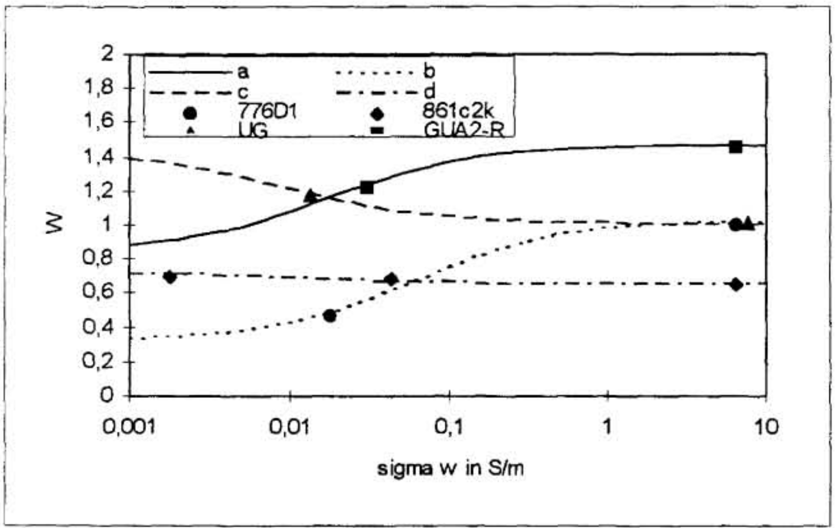

Figure 7 Anisotropy ratio W vs. water conductivity, experimental values and fitting curves.

Conclusions

Microcracks in crystalline rocks were described using well known structural parameters like formation factor and surface area-to-porosity-ratio. It was found that relationships between conductivity components and these parameters as well as the water composition show a similar behaviour to shaly sands. On this basis the experimentally measured frequency dependence for water saturated rocks was described with a relatively simple petrophysical model, which includes a electrolytic volume conductivity and a interface conductivity with an ohmic and a capacitiv contribution. The analyse of the complex electrical anisotropy behaviour of the crystalline rocks shows a significant dependence of anisotropy on water conductivity. In the range of low conductivity of the crack filling water electrical anisotropy is determined by direction dependent interface properties and the constrictivity of cracks. At high water conductivities the formation factor ratio and tortuosity determines electrical anisotropy. These behavior results in different types of anisotropy vs. water conductivity curves. The analyse may be used to distinguish cracks caused by different origin.

Acknowledgements
We want to thank the Deutsche Forschungsgemeinschaft for the support of our investigation. We also thank the team of the laboratory of the Dresden Groundwater Research Centre for the support of four years experimental work.

References
ARCHIE, G.E. (1942) The electrical resistivity log as an aid in determining some reservoir characteristics. Transactions of the American Institute of Mining, Metallurgical and Petroleum Engineers, 146, 54-62

BÖRNER, F., JUNG, F., SCHÖN, J. (1991): Complex electrical conductivity of KTB samples in the frequency range between 10-3 and 104 Hz - first results. Sientific Drilling, 2, 101-104.

BÖRNER, F.D. and SCHÖN, J.H. (1991) A relation between the quadrature component of electrical conductivity and the specific surface area of sedimentary rocks. The Log Analyst, 32, 612-613.

BÖRNER, F.D. and SCHÖN, J.H. (1995) Low frequency complex conductivity measurements of microcrack properties. In: Suveys in Geophysics Vol. 16, No. 1, pp. 121-135.

JONSCHER, A.K. (1981) A new understanding of the dielectric relaxation of solids.Journal of Material Sciences, 16,2037-2060

KULENKAMPFF, J., BÖRNER, F. und SCHOPPER, J.R. (1993): Broad band complex conductivity laboratory measurements enhancing the evaluation of reservoir properties. Trans. of the 15th Europ. Form. Evaluation Symp., Stavanger, Paper A.

LOCKNER, D.A. and BYERLEE, J.D. (1985) Complex resistivity measurements of confined rock. Journal of Geophysical Research, 90, 7837-7847

NOVER, G. and WILL, G. (1991): Laboratory measurements on KTB core samples: zeta potential, permeability and density as a tool for detection of flow phenomena. Scientific Drilling 2, 90-100.

OLHOEFT, G.R. (1985) Low frequency electrical properties. Geophysics, 50, 2492-2503

PAPE, H., RIEPE, L. and SCHOPPER, J.R. (1987) Theory of self-similar network structures in sedimentary and igneous rocks and their investigation with microscopical and physical methods. Journal of Microscopy, 148, 121-147

PHAM, A.T., MARTYNTIV, O.F. and TRAN, L.D. (1995) Heterogeneity of fractured granite: Effects on petrophysical Properties and water saturation. SCA Conference Paper Number 9525.

RAUEN, A. and LASTOVICKOVA, L. (1995) Investigation of electrical anisotropy in the deep borehole KTB. In: Suveys in Geophysics Vol. 16, No. 1, pp. 37-46.

RINK, M., and SCHOPPER, J.R. (1974) Interface conductivity and its implication to electric logging. In Transactions of the 15th Annual Logging Symposium (London, 1974)

SCHÖN, J. (1996): Physical Properties of rocks: Fundamentals and Principles of Petrophysics, Handbook of Geophysical Exploration: Seismic Exploration, Vol. 18, Pergamon Press.

VINEGAR, H.J. and WAXMAN, M.H. (1984) Induced Polarization of Shaly Sands. Geophysics 49, 1267-1287

WAXMAN, M.H. and SMITS, L.J.M. (1968) Electrical Conductivities in oil-bearing Shaly Sands. Society of Petroleum Engineers Journal, 243, 107-122